

This work was written as part of one of the author's official duties as an Employee of the United States Government and is therefore a work of the United States Government. In accordance with 17 U.S.C. 105, no copyright protection is available for such works under U.S. Law.

Public Domain Mark 1.0

<https://creativecommons.org/publicdomain/mark/1.0/>

Access to this work was provided by the University of Maryland, Baltimore County (UMBC) ScholarWorks@UMBC digital repository on the Maryland Shared Open Access (MD-SOAR) platform.

Please provide feedback

Please support the ScholarWorks@UMBC repository by emailing scholarworks-group@umbc.edu and telling us what having access to this work means to you and why it's important to you. Thank you.

Quantum-dot-induced transparency in a nanoscale plasmonic resonator

Xiaohua Wu, Stephen K. Gray, and Matthew Pelton*

Center for Nanoscale Materials, Argonne National Laboratory, 9700 S. Cass Ave., Argonne, Illinois 60439, USA

*pelton@anl.gov

Abstract: We investigate the near-field optical coupling between a single semiconductor nanocrystal (quantum dot) and a nanometer-scale plasmonic metal resonator using rigorous electrodynamic simulations. Our calculations show that the quantum dot produces a dip in both the extinction and scattering spectra of the surface-plasmon resonator, with a particularly strong change for the scattering spectrum. A phenomenological coupled-oscillator model is used to fit the calculation results and provide physical insight, revealing the roles of Fano interference and hybridization. The results indicate that it is possible to achieve nearly complete transparency as well as enter the strong-coupling regime for a single quantum dot in the near field of a metal nanostructure.

© 2010 Optical Society of America

OCIS codes: (160.4236) Nanomaterials; (250.5403) Plasmonics; (160.3918) Metamaterials; (350.4238) Nanophotonics.

References and links

1. M. Pelton, J. Aizpurua, and G. Bryant, "Metal-nanoparticle plasmonics," *Laser Photon. Rev.* **2**, 135–169 (2008).
2. X. Wu, Y. Sun, and M. Pelton, "Recombination rates for single colloidal quantum dots near a smooth metal film," *Phys. Chem. Chem. Phys.* **11**, 5867–5870 (2009).
3. J. Bellessa, C. Bonnand, J. C. Plenet, and J. Mugnier, "Strong coupling between surface plasmons and excitons in an organic semiconductor," *Phys. Rev. Lett.* **93**, 036404 (2004).
4. Y. Sugawara, T. A. Kelf, J. J. Baumberg, M. E. Abdelsalam, and P. N. Bartlett, "Strong coupling between localized plasmons and organic excitons in metal nanovoids," *Phys. Rev. Lett.* **97**, 266808 (2006).
5. W. Zhang, A. O. Govorov, and G. W. Bryant, "Semiconductor-metal nanoparticle molecules: Hybrid excitons and the nonlinear Fano effect," *Phys. Rev. Lett.* **97**, 146804 (2006).
6. R. D. Artuso and G. W. Bryant, "Optical response of strongly coupled quantum dot - metal nanoparticle systems: Double peaked Fano structure and bistability," *Nano Lett.* **8**, 2106–2111 (2008).
7. J. Khitrova, H. M. Gibbs, M. Kira, S. W. Koch, and A. Scherer, "Vacuum Rabi splitting in semiconductors," *Nat. Phys.* **2**, 81–90 (2006).
8. J. P. Reithmaier, G. Sek, A. Löffler, C. Hofmann, S. Kuhn, S. Reitzenstein, L. V. Keldysh, V. D. Kulakovskii, T. L. Reinecke, and A. Forchel, "Strong coupling in a single quantum dot - semiconductor microcavity system," *Nature* **432**, 197–200 (2004).
9. T. Yoshie, A. Scherer, J. Hendrickson, G. Khitrova, H. M. Gibbs, G. Rupper, C. Ell, O. B. Shchekin, and D. G. Deppe, "Vacuum Rabi splitting with a single quantum dot in a photonic crystal microcavity," *Nature* **432**, 200–203 (2004).
10. E. Peter, P. Senellart, D. Martrou, A. Lemaitre, J. Hours, J.-M. Gérard, and J. Bloch, "Exciton-photon strong-coupling regime for a single quantum dot embedded in a microcavity," *Phys. Rev. Lett.* **95**, 067401 (2005).
11. D. Englund, A. Faraon, I. Fushman, N. Stoltz, P. Petroff, and J. Vučković, "Controlling cavity reflectivity with a single quantum dot," *Nature* **450**, 857–861 (2007).
12. M. Fleishhauer, A. Imamoglu, and J. P. Narangos, "Electromagnetically induced transparency: Optics in coherent media," *Rev. Mod. Phys.* **77**, 633–673 (2005).
13. E. Waks and J. Vučković, "Dipole induced transparency in drop-filter cavity-waveguide systems," *Phys. Rev. Lett.* **96**, 153601 (2006).

14. V. Luk'yanchuk, N. I. Zheludev, S. A. Maier, N. J. Halas, P. Nordlander, H. Giessen, and C. T. Chong, "The Fano resonance in plasmonic nanostructures and metamaterials," *Nat. Mater.* **9**, 707–715 (2010).
15. M. Liu, T. W. Lee, S. K. Gray, P. Guyot-Sionnest, and M. Pelton, "Excitation of dark plasmons in metal nanoparticles by a localized emitter," *Phys. Rev. Lett.* **102**, 107401 (2009).
16. P. Palinginis, S. Tavenner, M. Lonerger, and H. Wang, "Spectral hole burning and zero phonon linewidth in semiconductor nanocrystals," *Phys. Rev. B* **67**, 201307 (2003).
17. S. A. Empedocles, D. J. Norris, and M. G. Bawendi, "Photoluminescence spectroscopy of single CdSe nanocrystallite quantum dots," *Phys. Rev. Lett.* **77**, 3873–3876 (1996).
18. A. Trugler and U. Hohenester, "Strong coupling between a metallic nanoparticle and a single molecule," *Phys. Rev. B* **77**, 115403 (2008).
19. C. de M. Donega and R. Koole, "Size dependence of the spontaneous emission rate and absorption cross section of CdSe and CdTe quantum dots," *J. Phys. Chem. C* **113**, 6511–6520 (2009).
20. P. Kukura, M. Celebrano, A. Renn, and V. Sandoghdar, "Imaging a single quantum dot when it is dark," *Nano Lett.* **9**, 926–929 (2009).
21. S. A. Empedocles and M. G. Bawendi, "Influence of spectral diffusion on the line shapes of single CdSe nanocrystallite quantum dots," *J. Phys. Chem. B* **103**, 1826–1830 (1999).
22. S. H. Park, M. P. Casy, and J. P. Falk, "Nonlinear optical properties of CdSe quantum dots," *J. Appl. Phys.* **73**, 8041–8045 (1993).
23. M. Liu, P. Guyot-Sionnest, T. W. Lee, and S. K. Gray, "Optical properties of rodlike and bipyramidal gold nanoparticles from three-dimensional computations," *Phys. Rev. B*, **76**, 235428 (2007).
24. P. B. Johnson and R. W. Christy, "Optical constants of the noble metals," *Phys. Rev. B* **6**, 4370–4379 (1972).
25. A. Taflov and S. C. Hagness, *Computational Electrodynamics: The Finite-Difference Time-Domain Method, 2nd Ed.* (Artech House, Boston, 2000).
26. J. M. Montgomery, T.-W. Lee, and S. K. Gray, "Theory and modeling of light interactions with metallic nanostructures," *Phys. Condens. Matter* **20**, 323201 (2008).
27. C. L. G. Alzar, M. A. G. Martinez, and P. Nussenzveig, "Classical analog of electromagnetically induced transparency," *Am. J. Phys.* **70**, 37–41 (2002).
28. N. Liu, L. Langguth, T. Weiss, J. Kastel, M. Fleischhauer, T. Pfau, and H. Giessen, "Plasmonic analogue of electromagnetically induced transparency at the Drude damping limit," *Nat. Mater.* **8**, 758–762 (2009).
29. C. F. Bohren, and D. R. Huffman, *Absorption and Scattering of Light by Small Particles, 2nd Ed.*, (Wiley, New York, 1983).
30. A. Nitzan and L. E. Brus, "Theoretical model for enhanced photochemistry on rough surfaces," *J. Chem. Phys.* **75**, 2205–2214 (1981).
31. J. Gersten and A. Nitzan, "Spectroscopic properties of molecules interacting with small dielectric particles," *J. Chem. Phys.* **75**, 1139–1152 (1981).
32. P. Nagpal, N. C. Lindquist, S. Oh, and D. J. Norris, "Ultrasoft patterned metals for plasmonics and metamaterials," *Science* **325**, 594–597 (2009).
33. L. E. Ocola, "Nanoscale geometry assisted proximity correction for electron beam direct write lithography," *J. Vac. Sci. Technol. B* **27**, 2569–2571 (2009).
34. Y. Cui, M. T. Bjork, J. A. Liddle, C. Sönnichsen, B. Boussert, and A. P. Alivisatos, "Integration of colloidal nanocrystals into lithographically patterned devices," *Nano Lett.* **4**, 1093–1098 (2004).

1. Introduction

Placing an optical emitter near a metal nanostructure can strongly modify the lifetime and efficiency of the emitter, due to the strong local electromagnetic fields associated with excitation of surface plasmons in the metal [1–6]. Semiconductor nanocrystals, or quantum dots (QDs), can exhibit such effects particularly clearly, due to their large dipole moments and photostability [2]. When the interaction between the QDs and the metal is strong enough, not only the emission properties of the QD but also the spectral properties of the surface-plasmon structure can be modified [3, 4]. To date, such strong coupling strengths have been achieved only by using a large number of QDs that couple coherently to a single plasmonic structure and produce a large collective effect. Highly intense incident fields can also effectively increase the coupling strength, and modified lineshapes and optical bistability have been predicted for a single QD coupled to a metal nanoparticle in the strong-field limit [5, 6].

Qualitatively new phenomena, though, are expected to arise if the hybrid QD / metal-nanoparticle structures can be optimized and modified lineshapes obtained using a single QD [7]. Such effects have already been obtained for epitaxial QDs coupled to monolithic op-

tical microcavities [8–10]. In particular, a single QD can produce a transparency dip in the reflectivity spectrum of a microcavity [11], an effect analogous to electromagnetically-induced transparency [12] and thus dubbed “dipole-induced transparency” (DIT) [13]. Compared to dielectric microcavities, plasmonic nanoresonators have stronger damping (*i.e.*, lower quality factors); this disadvantage, though, is at least partially compensated by the smaller mode volumes that surface plasmons enable. Indeed, since plasmonic resonators are not constrained by the diffraction limit, the dimensions of the entire QD / metal-nanoparticle hybrid system can be on the nanometer scale. This, in turn, opens up the possibility of using bottom-up synthesis and assembly to produce these systems as well as the possibility of integration with other plasmonic systems such as waveguides.

Transparency dips have also been induced in plasmonic resonances by coupling a relatively narrow, dark plasmon mode to a broader, bright mode [14]. This “plasmon-induced transparency” can produce very strong modulation but does not offer the possibility of active control. Transparency in the QD / metal-nanoparticle system, by contrast, can be switched simply by bleaching the QD transition; this could be accomplished by pumping the QD optically or by injecting charges electrically.

We investigate here the coupling between a single QD and a single plasmonic resonator formed by a pair of metal nanoparticles using rigorous electrodynamic simulations based on the finite-difference time-domain method. These nanoparticles have a small gap between them, where the optical fields are greatly enhanced and where the QD is located. Using realistic optical properties and dimensions for the QD and the metal nanoparticles, we calculate the extinction and scattering spectra of the QD / metal-nanoparticle hybrid structure. Our numerical simulations indicate that the QD induces a transparency dip in the surface-plasmon spectrum for both extinction and scattering, with the scattering spectrum having a deeper dip. Both spectra can be described phenomenologically using a classical coupled-oscillator model that includes the effects of both Fano interference and mode hybridization. Comparing the calculation and the fitting, we determine the coupling strength, g . We show that the strong-coupling or hybridization criterion, $2g > \gamma_{SP}$, where γ_{SP} is the SP resonance linewidth [7], may be fulfilled for realistic QD-SP hybrid structures.

2. Simulation method

As a model QD system, we consider CdSe nanocrystals. Although epitaxial QDs offer narrow linewidths at low temperatures and are generally free of blinking or spectral diffusion, they are difficult to incorporate into plasmonic structures at desired positions; by contrast, spherical nanocrystals are commonly synthesized colloiddally and could be integrated into lithographically fabricated metal structures by guided deposition, or could be chemically assembled together with colloidal metal nanoparticles. Nanocrystals also provide broad energy tunability, by changing their size and composition, allowing their transitions to match nearly any desired plasmon resonance.

Unlike previous work, where the QD was treated as a point dipole [15], here we take into account realistic dimensions for the semiconductor nanocrystal. Specifically, the QD diameter is adjusted to match the size that would be required in practice to produce a ground-state transition at the desired frequency, ω_{QD} . We treat the QD as a dielectric particle, with a dielectric function that reproduces the ground-state absorption by the quantum dot; QD emission, in particular, is not considered in our model. We ignore all higher-order transitions, modeling the dielectric function of the QD as a single Lorentzian:

$$\epsilon_{QD}(\omega) = \epsilon_{\infty-\text{CdSe}} - f \frac{\omega_{QD}^2}{\omega^2 - \omega_{QD}^2 + i\gamma_{QD}\omega}, \quad (1)$$

where $\epsilon_{\infty-\text{CdSe}}$ is the bulk CdSe dielectric constant at high frequency, f is the oscillator strength, and γ_{QD} is the transition linewidth. This corresponds to cryogenic conditions, where the linewidth is narrow and the ground-state transition is well isolated spectrally from higher-order transitions, which can therefore be ignored.

Homogeneous linewidths as narrow as 6 - 120 μ eV have been reported for CdSe QDs at liquid-helium temperatures [16, 17]. Room-temperature homogeneous linewidths, on the other hand, are approximately 25 meV; cooling the sample to some particular temperature should thus make it possible to obtain any desired linewidth between 0.1 and 25 meV. Although narrower linewidths lead to stronger transparency effects, as discussed below, the required computational time increases as the assumed linewidth decreases. We therefore set the single-dot linewidth in our calculations between 2 and 10 meV. We also use realistic oscillator strengths for the QD transition, in contrast to previous calculations [18]. Specifically, we use $f \approx 0.1$, determined by matching the spectrally integrated absorption per QD to experimentally measured values on QD ensembles with known concentrations [19]. The two-dimensional dipole of the CdSe QD is not explicitly considered. We also ignore blinking, which produces large fluctuations in the emission intensity from individual QDs but is not believed to correspond to changes in the absorption cross-section [20]. Spectral diffusion will broaden the transition on long time scales, but is negligible at low temperatures for integration times up to several minutes [21].

This classical model of the QD transition applies in the low-excitation limit, when quantum-mechanical coherences between the QD ground state and excited state and depletion of the QD ground state can be neglected. In other words, our results apply for optical intensities at the QD much lower than the saturation intensity for the QD transition. The saturation intensity for a CdSe QD is approximately 60 MW/cm² [22]; however, according to our simulations, the metal nanostructures enhance the field at the QD location by a factor of as much as 10⁴. Our calculations should thus be valid for incident intensities less than about 6 kW/cm².

The dielectric function of the metal is treated using a realistic (Lorentz-Drude) model [23]:

$$\epsilon_{\text{Ag}}(\omega) = \epsilon_{\infty-\text{Ag}} - \frac{\omega_D^2}{\omega^2 + i\omega\gamma_D} - \sum_{k=1}^N \frac{\sigma_{L,k}\omega_{L,k}^2}{\omega^2 - \omega_{L,k}^2 + i\gamma_{L,k}\omega}, \quad (2)$$

where $\epsilon_{\infty-\text{Ag}}$ is the material dielectric constant at high frequency, ω_D is the Drude frequency, and $\sigma_{L,k}$, $\omega_{L,k}$, and $\gamma_{L,k}$ are the strength, center frequency, and linewidth, respectively, of the k th resonance in the metal response. We use $N = 2$ Lorentzian terms and adjust the parameters in order to provide a good fit to experimental values for the complex dielectric function in the energy range from 1.6 eV to 3.7 eV [24].

Absorption and scattering spectra are calculated using rigorous finite-difference time-domain (FDTD) simulations [25, 26]. A time-windowed plane wave, with polarization along the spheroid major axes, is incident on the structure, where it is absorbed and scattered. The plane where the wave is generated defines the interface between the total-field and scattered-field regions, as illustrated in Fig. 1. The absorption spectrum is obtained by taking the Fourier transform of the flux through a three-dimensional box around the structure in the total-field region, and the scattering spectrum is obtained by taking the Fourier transform of the flux through a three-dimensional box around the structure in the scattered-field region. Extinction is simply calculated as the sum of absorption and scattering.

3. A single quantum dot coupled to a pair of silver ellipsoids

We first consider a silver spheroid dimer with a quantum dot in its gap, as shown in Fig. 1. The spheroids are 40 nm long with 5 nm radii and are aligned along their major axes with an edge-to-edge separation of 6 nm. A 4 nm spherical CdSe QD is positioned at the center of the

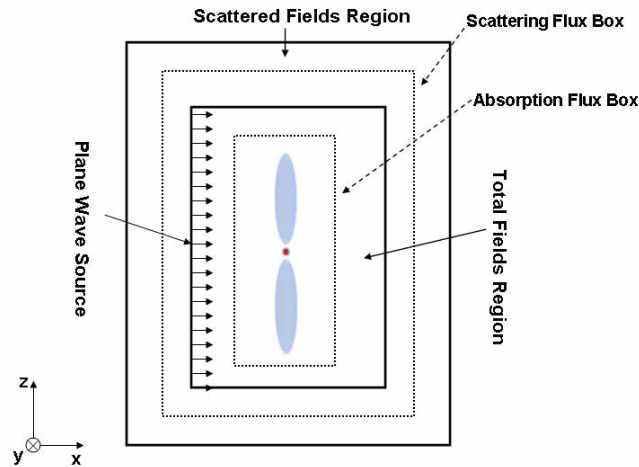


Fig. 1. Illustration of the quantum-dot / metal-nanoparticle hybrid system considered. The blue ellipses represent silver nanoparticles and the red circle represents a semiconductor nanocrystal. The various domains used in the finite-difference time-domain simulations are also illustrated.

gap between the two metal nanoparticles. The surrounding background material is taken to be air, and the calculation is performed with a grid size of 0.5 nm.

Figure 2 shows the calculated extinction and scattering spectra for this QD / metal-nanoparticle structure for two different QD transition linewidths, $\gamma_{QD} = 10$ meV and 2 meV. In the absence of QD absorption ($f = 0$), the structure shows a single broad SP resonance. With QD absorption ($f = 0.1$), by contrast, a transparency dip appears in both extinction and scattering spectra. The asymmetry of the spectra arises simply because the assumed QD transition frequency is slightly detuned from the plasmon resonance frequency. The depth of the dip depends on the QD transition linewidth, with a deeper dip for narrower γ_{QD} . It can also be seen that the scattering spectrum shows a deeper dip than the extinction spectrum. For the QD with a 2-meV linewidth, the transparency is nearly complete, with 94% of the metal-nanoparticle scattering canceled by the QD.

4. Fitting with a coupled-oscillator model

It is perhaps counterintuitive that the QD and metal nanoparticles, which are each absorptive, can become nearly transparent when coupled together. Moreover, the single QD is able to nearly cancel the surface-plasmon absorption even though its absorption cross-section is five orders of magnitude smaller than that of the metal nanostructure; this can be attributed to the strong local enhancement of the optical fields, and thus the greatly enhanced coupling strength, provided by the plasmonic nanostructure. In order to provide physical insight into this quantum-dot-induced transparency [13], we fit the rigorous calculation results using a phenomenological coupled-oscillator model. In this model, which has previously been used to describe electromagnetically induced transparency [27] as well as plasmon-induced transparency [28], the surface-plasmon resonance and the QD ground-state transition are each described as damped harmonic oscillators. These oscillators represent the polarization of the metal nanostructures and the semiconductor nanoparticle, respectively. They are coupled together through the electric near field with

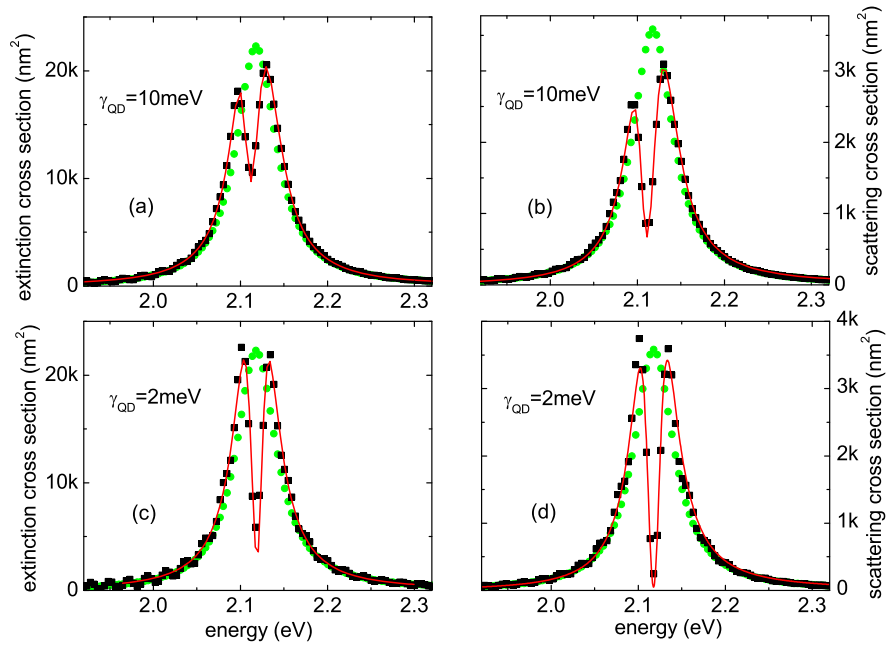


Fig. 2. Extinction and scattering spectra for a quantum-dot / metal-nanoparticle hybrid system. The structure is illustrated in the inset of (a). Solid squares are values of (a) extinction cross-section (in thousands of nm²) for quantum-dot linewidth $\gamma_{QD} = 10$ meV, (b) scattering cross-section for $\gamma_{QD} = 10$ meV, (c) extinction for $\gamma_{QD} = 2$ meV, and (d) scattering for $\gamma_{QD} = 2$ meV, all calculated using a rigorous finite-difference time-domain (FDTD) method. The solid lines are fits to a phenomenological coupled-oscillator model [Eq. (7) and Eq. (8)]. Solid circles are extinction and scattering spectra for the same system but without quantum-dot absorption, also calculated by the FDTD method.

coupling strength g . The equations of motion for the two oscillators are thus

$$\ddot{x}_{SP}(t) + \gamma_{SP}\dot{x}_{SP}(t) + \omega_{SP}^2 x_{SP}(t) + g\dot{x}_{QD}(t) = F_{SP}(t), \quad (3)$$

$$\ddot{x}_{QD}(t) + \gamma_{QD}\dot{x}_{QD}(t) + \omega_{QD}^2 x_{QD}(t) - g\dot{x}_{SP}(t) = F_{QD}(t), \quad (4)$$

where x_{SP} and x_{QD} represent the coordinates of surface-plasmon and QD oscillation, respectively, and F_{SP} and F_{QD} represent the normalized forces driving motion of these coordinates due to the external electromagnetic field. Since the QD extinction by itself is negligible compared to that of the metal nanostructure, $F_{QD}(t) \ll F_{SP}(t)$, and we set $F_{QD}(t) \approx 0$. We note that this classical coupled-oscillator model is intended only as a phenomenological description of the real physical situation, which is described more rigorously by the FDTD calculations. It can be shown to be equivalent to a quantum-mechanical description of a resonator (representing the plasmonic nanostructure) coupled to a two-level system (representing the QD), provided the QD is weakly excited, so that the majority of its population remains in the ground state [13].

For incident light with a given frequency ω , the driving force is $F_{SP}(t) = \text{Re}(F_{SP}e^{-i\omega t})$. At

steady state, both $x_{SP}(t)$ and $x_{QD}(t)$ will follow this driving frequency, and

$$x_{SP}(t) = \text{Re} \left(\frac{(\omega_{QD}^2 - \omega^2 - i\gamma_{QD}\omega)F_{SP}(t)}{(\omega^2 - \omega_{SP}^2 + i\gamma_{SP}\omega)(\omega^2 - \omega_{QD}^2 + i\gamma_{QD}\omega) - \omega^2 g^2} \right), \quad (5)$$

$$x_{QD}(t) = \text{Re} \left(\frac{-ig\omega F_{SP}(t)}{(\omega^2 - \omega_{SP}^2 + i\gamma_{SP}\omega)(\omega^2 - \omega_{QD}^2 + i\gamma_{QD}\omega) - \omega^2 g^2} \right). \quad (6)$$

The extinction of the incident light wave can be calculated as the work done by the external force:

$$C_{ext}(\omega) \propto \langle F_{SP}(t)\dot{x}_{SP}(t) \rangle \propto \omega \text{Im} \left(\frac{(\omega_{QD}^2 - \omega^2 - i\gamma_{QD}\omega)}{(\omega^2 - \omega_{SP}^2 + i\gamma_{SP}\omega)(\omega^2 - \omega_{QD}^2 + i\gamma_{QD}\omega) - \omega^2 g^2} \right), \quad (7)$$

where the angle brackets represent the average over an oscillation period. This represents the total extinction cross-section of the structure, including both absorption and scattering, provided the surface-plasmon linewidth γ_{SP} also includes both absorption and scattering. We therefore use Eq. (7) to fit the calculated extinction spectra; as shown in Figs. 2(a) and 2(c), excellent fits are obtained. The QD frequency and linewidth ($\omega_{QD} = 2.11$ eV and $\gamma_{QD} = 10$ or 2 meV)

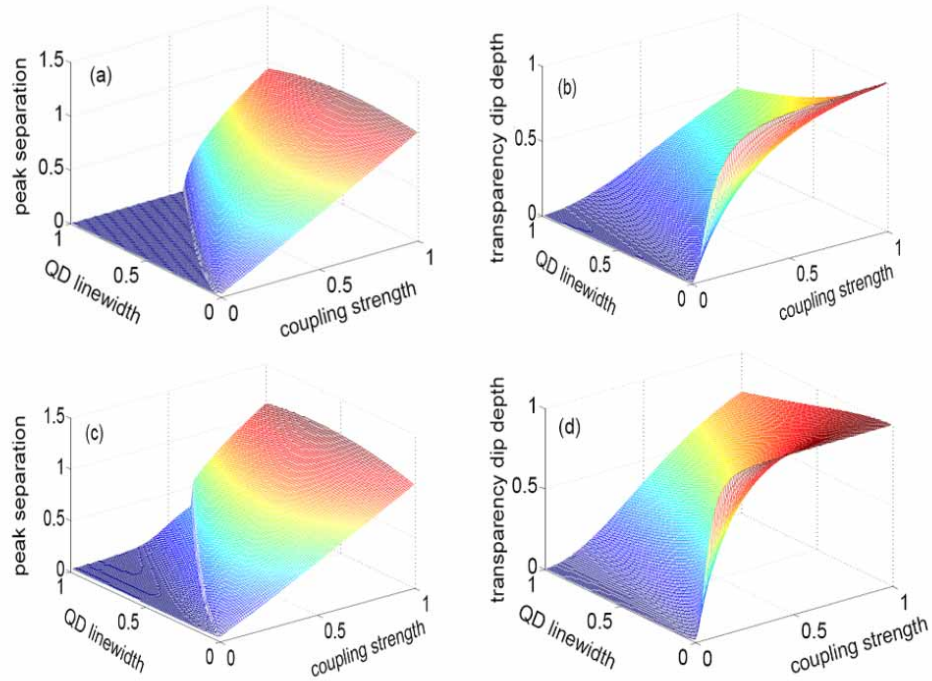


Fig. 3. (a) and (c): Peak-to-peak separation for extinction and scattering spectra, respectively, according to a coupled-oscillator model [Eq. (9) and Eq. (10)]. Values are shown as a function of quantum-dot linewidth, γ_{QD} , and coupling strength, g , with both values normalized by the surface-plasmon linewidth, γ_{SP} . (b) and (d) Depth of the transparency dip in the extinction and scattering spectra, normalized by the height of the plasmon-resonance peak, according to the same coupled-oscillator model.

are input parameters into the FDTD calculations, and are thus fixed constants in the fitting. The surface plasmon frequency and linewidth ($\omega_{SP} = 2.118$ eV and $\gamma_{SP} = 55.7$ meV) are obtained from a separate FDTD calculation without QD absorption ($f = 0$). The only remaining variable fitting parameters are the coupling strength, g , and an overall scaling factor. The fits can thus be used as a means of determining g ; we obtain $g = 26.4$ meV when $\gamma_{QD} = 10$ meV and $g = 28$ meV when $\gamma_{QD} = 2$ meV. This coupling strength is smaller than that achievable in plasmon-induced transparency, where coupling greater than 150 meV has been measured between different plasmon modes [28]; on the other hand, it is greater than that achievable in microcavity systems, where g is less than 1 meV [8–10].

Although extinction is usually measured for nanoparticle ensembles, it is generally more straightforward to measure scattering for single nanostructures [1]. Although the coupled-oscillator model does not provide a simple formula, in general, for the scattering cross-section, it can easily be calculated in the quasi-static limit, when the dimensions of the structure are small compared to the optical wavelengths [29]. In this limit, the extinction cross-section is $C_{ext} = 4\pi k \text{Im}(\alpha)$, where $k = \omega n/c$ is the wavevector of light and α is the polarizability of the nanostructure. Substituting this expression into Eq. (7), we find $\alpha \propto F_{SP}x_{SP}$. We can thus express the scattering cross-section as

$$C_{sca}(\omega) = \frac{8\pi}{3} k^4 |\alpha|^2 \propto \omega^4 \left| \frac{(\omega_{QD}^2 - \omega^2 - i\gamma_{QD}\omega)}{(\omega^2 - \omega_{SP}^2 + i\gamma_{SP}\omega)(\omega^2 - \omega_{QD}^2 + i\gamma_{QD}\omega) - \omega^2 g^2} \right|^2. \quad (8)$$

Equation (8) can be used to fit the scattering spectrum, and the results are shown in Figs. 2(b) and 2(d). These fits give $g = 26.7$ meV for $\gamma_{QD} = 10$ meV and $g = 29$ meV for $\gamma_{QD} = 2$ meV, in very good agreement with the values obtained by fitting the extinction spectra.

We note that it is possible to solve Eqs. (3) and (4) numerically to arbitrary precision, without needing to make the approximation $F_{QD} = 0$. The resulting spectra turn out to be nearly identical to the approximate ones shown in Fig. 2. There can be differences in more detailed aspects; for example, the approximate equations result in the SP and QD oscillators being, in general, out of phase, while the exact solution shows that the two oscillators are always exactly in phase.

We also note that other linearly coupled oscillator models could be used instead. For example, rather than being coupled through derivative terms, as in Eqs. (3) and (4), the oscillators can be coupled through terms proportional to the coordinates, x_{QD} and x_{SP} ; this would represent a simplified version of the coupled-dipole models discussed by Nitzan, Brus, and Gersten [30,31]. It is straightforward to derive relations between the prefactors for these alternative coupling terms and the coupling rate, g , employed in Eqs. (3) and (4). We have carried out calculations using this alternative coupling, and have obtained nearly identical results for the extinction and scattering spectra. The behavior demonstrated in this manuscript is thus likely generic to coupled-oscillator systems.

Equation (7) and Eq. (8) can be further simplified when the QD is resonant with the surface plasmon, *i.e.*, for $\omega_{QD} = \omega_{SP} = \omega_0$. Within the plasmon resonance peak, $\omega - \omega_0 \ll \omega_0$, giving

$$C_{ext}(\omega) \approx \omega \text{Im} \left(\frac{\omega_0 - \omega - i\gamma_{QD}\omega/2}{2\omega_0 \sqrt{g^2 - (\gamma_{SP} - \gamma_{QD})^2/4}} \left(\frac{1}{\omega - \Omega_+} - \frac{1}{\omega - \Omega_-} \right) \right), \quad (9)$$

$$C_{sca}(\omega) \approx \omega^4 \left| \frac{\omega_0 - \omega - i\gamma_{QD}\omega/2}{2\omega_0 \sqrt{g^2 - (\gamma_{SP} - \gamma_{QD})^2/4}} \left(\frac{1}{\omega - \Omega_+} - \frac{1}{\omega - \Omega_-} \right) \right|^2, \quad (10)$$

where $\Omega_{\pm} \equiv \omega_0 + i(\gamma_{SP} + \gamma_{QD})/4 \pm \sqrt{g^2/4 - (\gamma_{SP} - \gamma_{QD})^2/16}$. Inspection of these two expressions shows that both Fano-like interference and mode hybridization are responsible for the appearance of the transparency dip in the plasmon spectrum. When $g \ll (\gamma_{SP} - \gamma_{QD})/2$, the

spectrum can be understood as the result of interference between two resonances with the same frequency but with very different linewidths, often referred to as Fano interference [14]. When $g \gg (\gamma_{SP} - \gamma_{QD})/2$, hybridization results in the formation of two normal modes with different frequencies Ω_{\pm} and with the same linewidth $(\gamma_{SP} + \gamma_{QD})/2$. For emitters coupled to optical microcavities, this is known as the “strong-coupling” regime [7]. Fitting the calculated spectra to the coupled-oscillator model therefore makes it possible to determine whether the system is in the weak- or strong-coupling regime, and thus which phenomenon (interference or hybridization) is responsible for the observed transparency. For the hybrid structure consisting of a QD between two silver spheroids, we find that the system is in the weak-coupling regime ($g < \gamma_{SP}/2$) when $\gamma_{QD} = 10$ meV, and is at the onset of the strong-coupling regime ($g > \gamma_{SP}/2$) when $\gamma_{QD} = 2$ meV. In both cases, the system is near the threshold between the two regimes, meaning that Fano-like interference and mode splitting are both playing an important role in determining the calculated line shape.

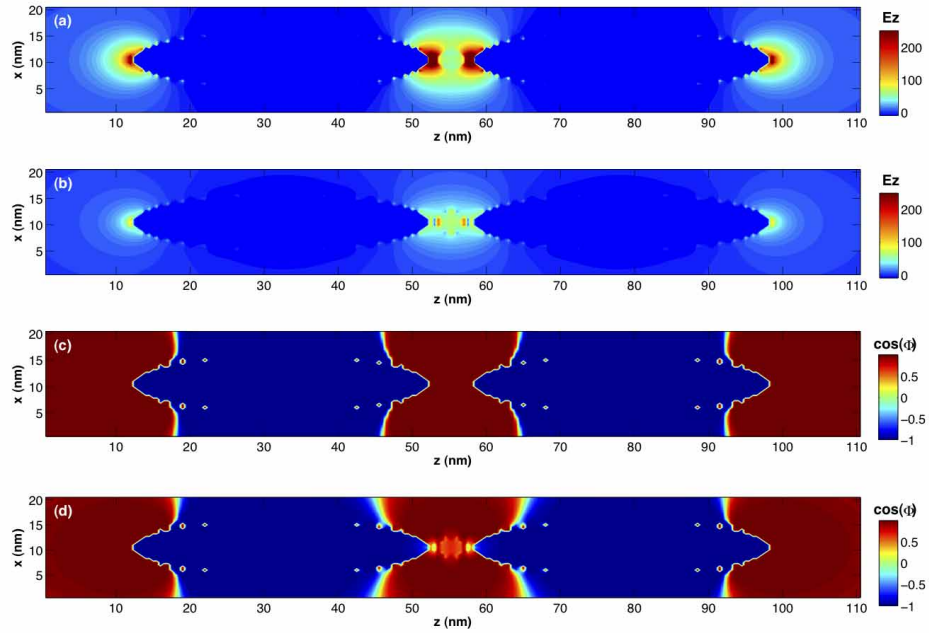


Fig. 4. Electric field, E_z , and cosine of its phase, $\cos(\Phi)$, for the quantum-dot / metal-nanoparticle structure shown in Fig. 1, calculated using the rigorous finite-difference time-domain method. The z direction is along the long axes of the metal nanoparticles. Results are shown at the surface-plasmon resonance energy with (b,d) and without (a,c) the quantum-dot absorption.

The coupled-oscillator model thus provides insight into the physical phenomena responsible for the predicted QD-induced transparency; it also gives guidelines for maximizing the effect. In particular, Eqs. (9) and (10) show that wider and deeper transparency dips can be obtained by reducing the QD linewidth, γ_{QD} . This is illustrated in Figure 3, where we show the transparency dip depth and peak separation as a function of γ_{QD} and g (for a fixed γ_{SP}). It can be seen that, for a narrower QD linewidth, a lower coupling strength is required to open up a transparency dip in the extinction spectrum; similarly, for a given coupling strength, a narrower QD linewidth leads to more complete transparency. A similar but more dramatic tendency exists in the scat-

tering spectrum. Narrowing the QD linewidth while keeping the total oscillator strength fixed means stronger maximum absorption at the QD resonance frequency, which in turn increases the coupling to the plasmonic structure and enhances the QD-induced transparency. Experimentally, this can be achieved simply by lowering the temperature of the system. A narrower surface-plasmon linewidth, γ_{SP} , will also benefit the QD-induced transparency. We note that any changes in γ_{SP} and γ_{QD} will affect the coupling strength, g , meaning that the parameters are interconnected and cannot be optimized independently.

To further understand the transparency effect in the QD / metal-nanoparticle structure, we return to the rigorous FDTD calculations, and investigate the field pattern at the surface-plasmon resonance frequency, ω_{SP} . Figure 4 shows the calculated distribution of E_z , the electric-field component along the long axes of the metal spheroids, and its phase. Without QD absorption ($f = 0$), a broad plasmon resonance is observed in the spectrum, and the field pattern corresponds to a dipole mode, with a clear π phase difference between the interior of the spheroids and the gap between them. For the structure with QD absorption ($f = 0.1$), a transparency dip appears around ω_{SP} , and the local field is greatly reduced. The decrease in the field is caused by destructive interference between the QD transition and the plasmon resonance, which is reflected in the large phase difference between the field within the QD and in the neighboring gap region.

5. Single quantum dot coupled to a realistic metal nanostructure

So far, our investigation has focused on a structure consisting of a pair of silver spheroids separated by a 6-nm gap that contains a single CdSe QD. Although it is not unrealistic to suppose that such a structure could eventually be produced through chemical synthesis and assembly, such a process would certainly be difficult. We therefore extend our considerations to a more realistic hybrid structure that could potentially be fabricated through a combination of top-down fabrication and bottom-up assembly. In particular, we consider a metal dimer consisting of two silver hexahedrons with a uniform rhomboid cross-section, or “nanodiamonds,” as illustrated in Fig. 5(a). The diagonal axes for each metal nanoparticle are 40 nm and 80 nm long, and the structures are 20 nm high. The sharp angles of each rhombus are rounded with a 5-nm radius of curvature, in order to mimic the rounding that occurs during fabrication. The dimer has a 10 nm edge-to-edge gap, with a QD positioned in the middle. The hybrid structure sits on a glass substrate ($\epsilon = 2.25$) in air. Although the metal-nanoparticle structure would be challenging to fabricate lithographically, it could likely be produced using state-of-the-art electron-beam lithography and template-stripping methods [32, 33]. The QD could be positioned in the gap using guided colloidal deposition [34].

Using the rigorous numerical simulation method, we calculate a resonance frequency, $\omega_{SP} = 2.112$ eV, and linewidth, $\gamma_{SP} = 144$ meV, for the metal nanostructure. This linewidth is larger than that of the previous metal nanostructure, because of the larger dimensions and the correspondingly larger radiative damping. In order to match the plasmon resonance, the QD diameter is set to 4 nm. As above, we use QD oscillator strength $f = 0.1$ and linewidth $\gamma_{QD} = 2$ meV; for these calculations, we use a grid size of 1 nm.

The extinction and scattering spectra for this structure, obtained using the FDTD calculations, are shown in Fig. 5(b) and 5(c), together with fits using the coupled-oscillator model. Compared to the spheroid dimer structure in Fig. 1, the QD-induced transparency is reduced due to the weaker coupling ($g = 9$ meV, by fitting to the coupled-oscillator model). If particles with sharper tips could be fabricated, a larger QD-induced transparency would be obtained. For example, Fig. 5 also shows the calculated spectra when the particles are rounded with a 2-nm radius of curvature. Since the sharper tips red-shift the plasmon resonance frequency, we have increased the QD diameter correspondingly, to 6 nm. In this case, fitting gives $g = 19$ meV. We

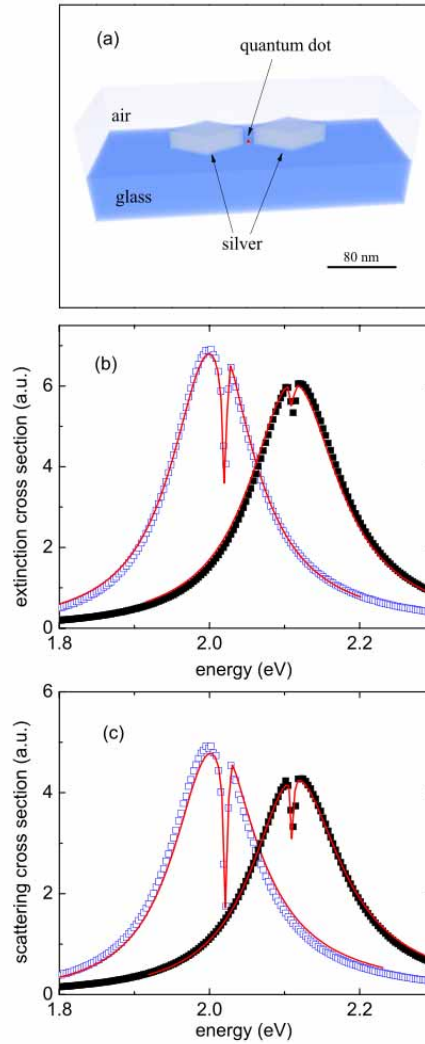


Fig. 5. (a) Illustration of a quantum-dot / metal-nanoparticle hybrid structure that could potentially be fabricated lithographically. (b) Extinction spectra for the structure when the corners of the metal nanoparticles have a radius of curvature of 5 nm (solid squares) and 2 nm (open squares), calculated using the rigorous finite-difference time-domain (FDTD) method. The lines are fits to Eq. (7). (c) Scattering spectra for the same structures, also calculated by the FDTD method. The lines are fits to Eq. (8).

note that the grid size used in the FDTD calculations limits the precision with which the QD diameter can be specified; this, in turn, limits the accuracy of the calculated coupling. We note also that no attempt has been made to optimize the metal-nanostructure geometry in order to maximize the induced transparency. The most significant limitation on the coupling strength, though, comes from the strong radiative damping of the plasmon resonance. Smaller metal nanostructures would have reduced radiative losses, but are probably not realistic to fabricate lithographically. Coupling to dark plasmon modes [15], on the other hand, should eliminate radiative losses and make it possible to achieve larger coupling strengths.

Even though realistic lithographic fabrication tolerances give a hybrid QD / metal-nanoparticle structure that is in the weak-coupling regime, meaning that no mode hybridization occurs, a significant transparency dip still exists in both the extinction and scattering spectra, leading to several potential applications. In particular, the scattering spectrum could readily be measured for such a structure using dark-field microscopy techniques. Fitting this spectrum to a coupled-oscillator model would allow the QD resonance frequency, ω_{QD} , and linewidth, γ_{QD} , to be determined, provided the plasmon spectrum is characterized independently in the absence of the QD. The hybrid structure thus provides a new method to measure the absorption spectra of individual QDs, which is otherwise a considerable challenge [20]. Alternatively, the QD / metal-nanoparticle system could serve as a fully nanoscale, all-optical modulator that could be integrated into plasmonic systems. Absorption of only two photons by the QD will saturate its transition, eliminating the transparency dip; because of the highly enhanced local field, the incident power required for this bleaching should be extremely low [11]. The same saturation effect would also modulate the strong dispersion at the transparency dip, allowing a collection of the structures to serve as a dynamically controllable slow-light medium.

6. Conclusions

In summary, we used rigorous electromagnetic simulations to calculate extinction and scattering spectra for a hybrid nanostructure consisting of a single semiconductor nanocrystal quantum dot and a metal-nanoparticle dimer. Because of the strong local field from the localized surface plasmon and the narrow transition linewidth of the QD at low temperature, a dramatic transparency dip appears in the broad plasmon resonance. This nearly complete transparency arises even though both structures are absorptive and even though the optical cross-section of the QD is five orders of magnitude lower than that of the metal nanostructure. This is possible because the excitation of plasmon resonances in the metal nanostructure strongly localizes electromagnetic fields at the position of the quantum dot, enhancing the coupling to the QD transition; this, in turn, leads to Fano interference and hybridization between the plasmon resonance and the QD transition. The transparency effect could be used in several applications, including the measurement of single-QD absorption spectra and the production of nanoscale plasmonic modulators.

Acknowledgements

Work at the Center for Nanoscale Materials was supported by the U. S. Department of Energy, Office of Science, Office of Basic Energy Sciences, under Contract No. DE-AC02-06CH11357. We thank Jason M. Montgomery, Tae-Woo Lee, and Lina Cao for help with FDTD programming.

The submitted manuscript has been created by UChicago Argonne, LLC, Operator of Argonne National Laboratory ("Argonne"). Argonne, a U.S. Department of Energy Office of Science laboratory, is operated under Contract No. DE-AC02-06CH11357. The U.S. Government retains for itself, and others acting on its behalf, a paid-up nonexclusive, irrevocable worldwide license in said article to reproduce, prepare derivative works, distribute copies to the public, and

perform publicly and display publicly, by or on behalf of the Government.